DELINEATION OF COAL FIRE RISK AREAS FROM LANDSAT-8 TIRS DATA: A CASE STUDY OF NA DUONG COALFIELD (NORTH-EAST OF VIETNAM)

Danh-tuyen VU[1], Tien-thanh NGUYEN[1], Anh-huy HOANG[2], Thi-thu-huong PHAM[1]

DOI: 10.21163/GT_2023.181.14

ABSTRACT:
Coal fires are a persistent threat to major coal-producing countries in the world. Thus, it is very important to delineate the potential risks of coal fires. This study presents a method for the delineation of coal fire risk areas from Landsat-8 TIRS data. Land surface temperatures (LSTs) were first retrieved from the Landsat-8 TIRS images. The degree of spatial autocorrelation among these LSTs was then identified using local Moran's *I* statistic. Thermal-related anomalies for the delineation of coal fire risk areas were identified by setting the MEAN+2*SDEV (SDEV is the standard deviation), MEAN+3*SDEV, and MEAN+4*SDEV formulas as thresholds on the local Moran's *I* statistic. These coal fire risk areas were finally validated using known coal fire sites and cross-validated by comparing them with those obtained from hot spot analysis. A case study of the Na Duong coal field (northern Vietnam) has shown that coal fire risks at moderate and high levels were mainly detected in the center of the coal field. The higher values of local Moran's *I* statistic, the higher levels of coal fire risks. These coal fire risks were mainly concentrated around known coal fire sites. These results reveal that Landsat-8 TIRS data can effectively delineate coal fire risk areas.

Key-words: *Land surface temperatures; coal fire risks; local Moran's I statistic; Na Duong coal field (Vietnam), Landsat-8 TIRS data.*

1. INTRODUCTION

Coal fires, which occur on the surface (primarily in coal waste piles) and in underground coal seams and are caused by spontaneous combustion, natural events (lightning, forest fires, and peat fires), and human activities (mining and domestic fires) (Du et al. 2015; Vu and Nguyen 2021a). These fires lead to the emission of greenhouse relevant and toxic gasses, the deterioration of vegetation, land subsidence due to volume loss underground, and to the loss of the valuable resource coal (Kuenzer et al. 2007). Coal fires pose potential risks to the environment, infrastructure, and human health. It is therefore, the delineation of coal fire risk areas plays an important role in controlling and preventing their effects and environmental impacts.

Coal fire risks have been conventionally conducted by temperature measurements in boreholes and using thermal cameras in the 1960s (Greene et al. 1969; Knuth et al. 1968) and 1970s (Ellyett and Fleming 1974; Rabchevsky 1972). Although, the main advantages of these methods are the ability of precise coal fire risk detection, they are nearly impossible to gather enough data over large area, especially for inaccessible areas. The occurrence of high spatial resolution airborne thermal remote sensing has overcome this limitation (Vu and Nguyen 2018). However, the high costs for data acquisition by these airborne scanners have limited their practical applications. Since freely available thermal infrared images acquired by satellite sensors started to become available, automated coal fire risk area delineation from space became easier (Künzer 2014). Recent evidence suggests that thermal infrared data from earth observation by satellites has proven to be a powerful tool to support the delineation of coal fire risks(Vu and Nguyen 2021a; Nguyen and Vu 2019b; Vu and Nguyen 2018). Thus, thermal infrared remotely sensed images were chosen to delineate coal fire risks in this study.

[1]*Faculty of Surveying, Mapping and Geographic Information, Hanoi University of Natural Resources and Environment, Vietnam, vdtuyen@hunre.edu.vn*, C*orresponding author: ntthanh@hunre.edu.vn, ptthuong.tdbd@hunre.edu.vn*
[2]*Faculty of Environment, Hanoi University of Natural Resources and Environment, Vietnam, hahuy@hunre.edu.vn*

The methods involved in the automated delineation of coal fire risk areas from thermal infrared sensed data typically incorporate the identification of changes in the surface feature and by-products of coal fires based on land surface temperatures. Using visible/near-infrared data, Song and Kuenzer (2017) successfully demarcated coal fire risks through the study of spectral reflectance (400-2500 nm) properties of coals, adjacent sediments, metamorphic and pyrometamorphic rocks in Wuda coal fire areas, northern China. Apart from thermal infrared data, short-wave infrared (SWIR) data covered by Landsat TM band 4, 5, and 7, ETM+ SWIR band 7, OLI band 6 and 7, and ASTER band 9 has been also successfully employed to detect coal fires in many coal fields around the world such as China's Rujigou coal field (Huo et al. 2014a; Huo et al. 2014b; Huo et al. 2015) and India's Jharia coalfield (Singh et al. 2017). However, up to now, far too little attention has been paid to the spatial autocorrelation among thermal infrared images-obtained land surface temperatures in the coal fire risk delineation. The spatial autocorrelation can be measured using spatial statistics such as Getis's *G*, Geary's *C*, spatial scan, and the Moran's *I* statistic (Nguyen et al. 2016; Nguyen and Vu 2019a; Nguyen 2017). Among these spatial statistics, the local Moran's *I* statistic has been the most commonly used for spatial autocorrelation analysis (Tiefelsdorf 2002). To overcome the limitation of commonly used methods for the detection of coal fire risks when the spatial pattern of LSTs is not taken into account, one of the first studies on this issue by (Nguyen and Vu 2019b) has attempted to take hot spot analysis-based spatial autocorrelation into the study of coal fires in the Khanh Hoa coal field, north-east of Vietnam. Later, with the help of the local Moran's *I* statistic, Vu and Nguyen (2021a) has also successfully identified spatial patterns of LSTs retrieved from remotely sensed data and their relation to coal fires in the Khanh Hoa coal field. The results of Vu and Nguyen (2021a) have shown that the closer the coal fire sites, the higher the spatial autocorrelation level, and there exists a strong degree of positive correlation between the distribution of LST spatial pattern with active coal fire sites. However, the main drawback of this study was the lack of detecting local Moran's *I* anomalies obtained from LSTs. It is therefore, to overcome this limitation, based on the idea of spatial autocorrelation among LSTs proposed by Vu and Nguyen (2021a), this study aims to delineate coal fire risk areas from Landsat-8 TIRS data using the local Moran's *I* statistic.

In this study, the first step of this method will retrieve LSTs from the Landsat-8 TIRS data using the radiative transfer equation. It will go on to identify the degree of spatial autocorrelation among these LSTs using the local Moran's *I* statistic. Thermal-related anomalies for the delineation of coal fire risk areas were then identified by setting the MEAN+2*SDEV (SDEV is the standard deviation), MEAN+3*SDEV and MEAN+4*SDEV formulas as thresholds on the local Moran's *I* statistic. These coal fire risks were finally validated using known coal fire sites.

2. STUDY AREA

The Na Duong basin is situated near the boundary between the Indochina and Southern China microplates. It is part of the Cao Bang Tien Yen fault system (Pubellier et al. 2003) which parallels the Ailao Shan-Red River Fault Zone at 160 km distance to the South (Madelaine et al. 2018). The Na Duong coal field, an open pit coal mine in the Na Duong basin, is situated in the Na Duong basin, Loc Binh district, approximately 20 km SE of Lang Son province, northern Vietnam (Ducrocq et al. 2015). Geographically, the study area of the Na Duong coal field is situated between 21°45′45″N to 21°43′50″N latitudes and 106°57′50″E to 106°59′40′E longitudes, covering an area of approximately 9.8 square kilometers (**Fig. 1**). Its coal reserve was estimated to be 17.5 million metric tons. The coal seams from the Na Duong coal pit represent mainly the telocollinite subfacies and originated mostly under conditions of a wet forest swamp with a high water level (Wysocka 2009). Na Duong coal is a rare special coal in Vietnam with the characteristics of being able to burn naturally, with a large sulfur content. When it meets water, this coal can be converted into sulfuric acid, if released into the environment, it will affect the environment, health, and the surrounding environment. A study of Hoang (2005) concluded that the working environment in the coal field was contaminated by toxins from the coal fires. Coal fires in the Na Duong coal field were reported in recent years. Particularly, the fire intensity was strong in 2017. Thus, remotely sensed images in this year were employed to delineate coal fire risk areas in the coal field.

3. DATA AND METHODS

3.1. Data

In this study, Landsat-8 TIRS data was used to delineate coal fire risk areas in the Na Duong coal field. The Landsat-8 images used in this study were the Level-1 precision and terrain-corrected product that was corrected geometrically and topographically through co-registration (Chen et al. 2017). The Landsat-8 image (path 127, row 045) distributed by the U.S. Geological Survey was acquired on December 6, 2017, and projected in the UTM Zone N48 and WGS 1984 ellipsoid datum. The image was almost free of clouds. The Na Duong coal fire boundary was provided by Na Duong VVMI coal company limited. In addition, a total of four active coal fire sites collected from the field survey by the retrospective study will be also used for the validation of coal fire risk area delineation (**Fig. 1**).

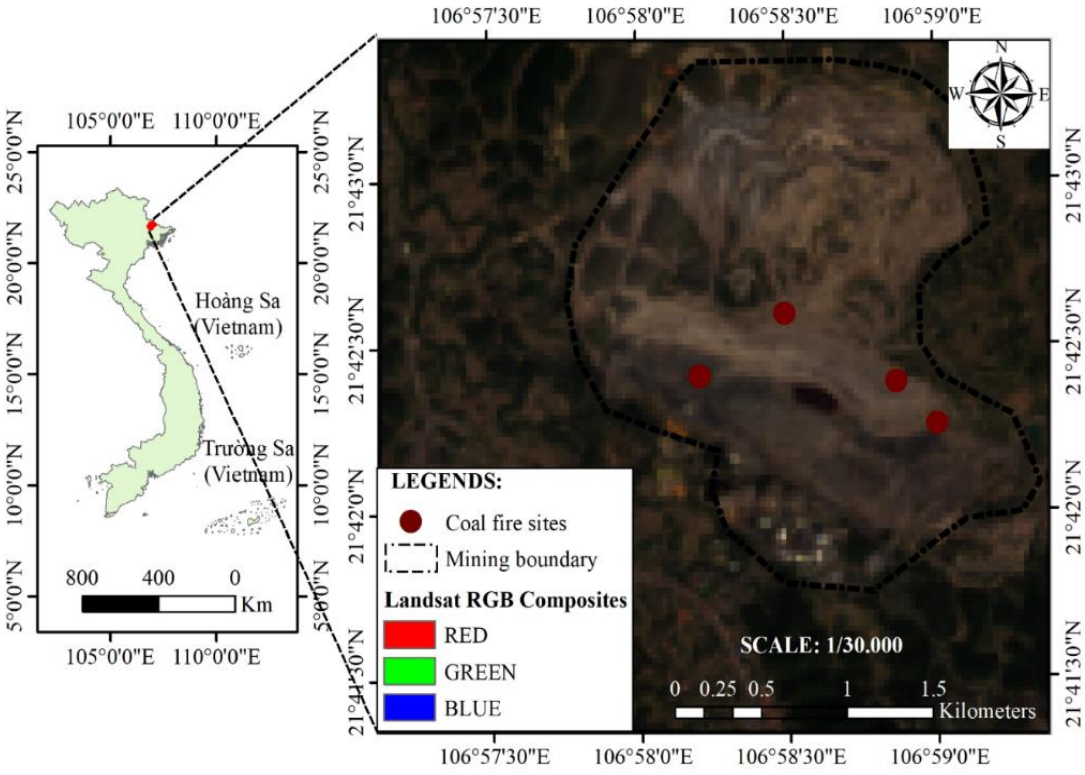

Fig. 1. Study area of Na Duong coal field, Lang Son province, north-east of Vietnam (natural color composite image of Landsat-8 OLI bands 4, 3, 2 in RGB).

3.2. Methods

In this study, the first step of this method will retrieve the land surface temperatures from the Landsat-8 TIRS data using the radiative transfer equation. The degree of spatial autocorrelation among these LSTs was then measured with the help of local Moran's *I* statistic. It will then go on to the identification of thermal-related anomalies for the delineation of coal fire risk areas by setting the MEAN+2*SDEV, MEAN+3*SDEV, and MEAN+4*SDEV formulas as thresholds on the local Moran's *I* statistic. These coal fire risks were validated using known coal fire sites. Finally, Landsat-8 TIRS images acquired in the Na Duong coal field (northern Vietnam) were used to identify low, moderate, and high levels of coal fire risks in the coal field.

a. Land surface temperature retrieval from Landsat-8 TIRS data

The top of atmosphere (TOA) spectral radiance using a conversion equation given as follows (Mishra et al. 2014):

$$L_{TOA,\lambda} = M_L \times Q_{cal} + A_L \quad (1)$$

where: $L_{TOA,\lambda}$ is the TOA radiance [W/(m²·sr·µm)] at the wavelength λ (µm) measured by the Landsat-8 OLI and TIRS1; M_L is the band-specific multiplicative rescaling; A_L is the band-specific additive rescaling factor; and Q_{cal} is the quantized and calibrated standard product pixel values [DN].

A radiative transfer equation can express the TOA radiance received by a sensor using the following equation (Barsi et al. 2003):

$$L_{TOA,\lambda} = \tau_\lambda\left[\varepsilon_\lambda B_{b,\lambda}(T_s) + (1-\varepsilon_\lambda)L^{\downarrow}_{atm,\lambda}\right] + L^{\uparrow}_{atm,\lambda} \quad (2)$$

where: $L_{TOA,\lambda}$ is the TOA radiance [W/(m²·sr·µm)] at the wavelength λ = 10.60-11.19µm measured by the Lansat-8 TIRS1; ε_λ is the land surface emissivity; $B_{b,\lambda}(T_s)$ is the blackbody radiance [W/(m²·sr·µm)] given by the Planck's law and T_s is the LST [Kelvin]; $L^{\uparrow}_{atm,\lambda}$ is the upwelling atmospheric radiance [W/(m²·sr·µm)]; $L^{\downarrow}_{atm,\lambda}$ is the downwelling atmospheric radiance [W/(m²·sr·µm)] and τ_λ is the total atmospheric transmissivity [dimensionless] between the surface and the sensor.

In this study, the land surface emissivity (LSE) was derived based on the work of (Sobrino et al. 2008) by using the Normal Differential Vegetation Index (NDVI)-based threshold approach. LSE of each land cover type is derived using vegetation fraction (f_v) determined from NDVI. The following equation is used to derive vegetation fraction from NDVI:

$$f_v = \left(\frac{NDVI - NDVI_s}{NDVI_v - NDVI_s}\right)^2 \quad (3)$$

where: $NDVI_s$ and $NDVI_v$ are the pixel values corresponding to non-vegetation cover (bare soil) and full vegetation cover, respectively.

For this present research, the values of $NDVI_s$ = 0.18 and $NDVI_v$ = 0.76 were extracted from the NDVI histogram using the 5% and 95% confidence levels of NDVI values as proposed by Sobrino et al. (2008). LSE values were calculated in three cases: (i) if $NDVI < NDVI_s$ then the pixel is considered mainly covered by bare soil ($f_v = 0$), and a mean value of 0.97 is assumed for the soil emissivity (ε_s) (Sobrino et al. 2008); (ii) if $NDVI > NDVI_v$ then the pixel corresponds to dense vegetation areas (fully vegetated) ($f_v = 1$), and the vegetation emissivity (ε_v) is given a value of 0.99 (Sobrino et al. 2008); (iii) if $NDVI_s < NDVI < NDVI_v$ then each pixel is considered mixing of bare soil and vegetation, and the emissivity can be derived from the following equation:

$$\varepsilon_i = f_v \cdot \varepsilon_v + (1 - f_v) \cdot \varepsilon_s \quad (4)$$

where: ε_i is the emissivity of pixel i; ε_v and ε_s are the vegetation and soil emissivity; and f_v is the vegetation fraction obtained from equation (3). The LST, T_s [Kevin], is estimated by inversion of Planck's law using equation (5):

$$T_s = \frac{K_2}{ln\left[\frac{K_1}{B_{b,\lambda}(T_s)} + 1\right]} \quad (5)$$

where: K_2 = calibration constant 2 [Kevin]; K_1 = calibration constant 1 [W/(m²·sr·µm)]; $B_\lambda(T_s)$ = blackbody radiance [W/(m²·sr·µm)]; and ln = natural logarithm.

b. Local Moran's I statistic

The spatial pattern of land surface temperatures at each specific location can be identified using the local Moran's *I* statistic. The local Moran's *I* statistic for the LST at location *i* is defined as the following equation (Anselin 1995):

$$I_i = \frac{(x_i - \bar{x})}{\sigma^2} \sum_{j\#i, j\in J_i}^{N} W_{ij}(x_j - \bar{x}) \quad (6)$$

where: x_i and x_j are LSTs at locations i and j; J_i denotes the neighbourhood set of LSTs at location i; $\bar{x}$ is the mean of land surface temperatures; W_{ij} is a spatial weight matrix used for computing a local Moran's I coefficient at the location i within a given distance d. W_{ij} is a spatial weight matrix for a given distance d and d_{ij} is the distance between the RMDs at locations i and j. If $d_{ij} < d$ then $W_{ij} = 1$ and $W_{ij} = 0$ otherwise.

In this way, only the pairs of sites (i, j) within the stated distance class (d) are taken into account in the calculation of any given coefficient. For a given distance class, the weights W_{ij} are written in a $(n \times n)$ spatial weighting matrix W_{ij}. Before computing the local Moran's, *I* coefficient, a matrix of geographic distances among land surface temperatures must be first calculated.

The value I_i = 0 indicates no spatial autocorrelation; I_i > 0 represents positive spatial autocorrelation; and if I_i < 0 then the spatial autocorrelation is negative. When there is a positive Moran's *I* coefficient, two types of LST spatial clusters were identified including high-high (H-H) clusters (a high LST surrounded by high LSTs) and low-low (L-L) clusters (a low LST surrounded by low LSTs). If $p(I_i)<\alpha$, $I_i>0$, and $x_i - \bar{x}>0$, then x_i and $x_{j\in Ji}$ belong to a spatial cluster between high LSTs (H-H clusters). If $p(I_i)<\alpha$, $I_i>0$ and $x_i - \bar{x}<0$, then x_i and $x_{j\in Ji}$ belong to a spatial cluster between low LSTs (L-L clusters). If $p(I_i)<\alpha$, $I_i<0$, and $x_i - \bar{x}>0$ then a high LST, x_i, is surrounded by low LSTs, $x_{j\in Ji}$, (H-L outliers). If $p(I_i)<\alpha$, $I_i<0$, and $x_i - \bar{x}>0$ then a low LST, x_i, is surrounded by high LSTs, $x_{j\in Ji}$, (L-H outliers) (Vu and Nguyen 2021a).

c. Identification of coal fire risk areas

The distribution of local Moran's *I* statistic is strongly right-skewed (Nguyen et al. 2016; Nguyen and Vu 2019a). Thus, thermal-related anomalies to delineate coal fire risk areas were identified by setting the MEAN+2*SDEV (SDEV is the standard deviation), MEAN+3*SDEV, and MEAN+4*SDEV formulas as thresholds on local Moran's *I* coefficients. Four classes of coal fire risks are obtained and ranked, accordingly, as follows: (i) no risk, if I_i < MEAN+2*SDEV; (ii) low risk, if MEAN+2*SDEV < I_i < MEAN+3*SDEV; (iii) moderate risk, if MEAN+3*SDEV < I_i < MEAN+4*SDEV; (iv) high risk, I_i > MEAN+4*SDEV.

d. Accuracy assessment

The areas of coal fire risks were first validated based on four coal fire sites collected from the field survey and then cross-validated by comparing them with those obtained from hot spot analysis. The validation was performed using ArcGIS software. In this case, the layer of coal fire sites is laid over that of coal fire risk areas which were obtained from the above-discussed method. The degree of spatial correlation or conformity between the areas of medium-to-high risk levels and the active coal fire sites is the basis for evaluating the accuracy of the proposed method. The higher the degree of spatial correlation or conformity, the higher the accuracy of the proposed method. The cross-validation was then carried out by comparing areas of coal fire risks at different levels delineated from the proposed method with those obtained from hot spot analysis. The Getis-Ord's G_i^* statistic-based hot spot analysis allows for identifying spatial clusters of high (hot spots) and low (cold spots) values at local locations (Kowe et al. 2019). Recently, a recent study of Nguyen and Vu (2019b) has successfully employed this method for detecting coal fires in the Khanh Hoa coal field in north-east of VietNam. Therefore, different coal fire risk levels delineated from hot spot analysis were also used to compare with those obtained from the proposed method.

4. RESULTS AND DISCUSSIONS

4.1. Distribution of LSTs in the Na Duong coal field

Land surface temperatures are indicative of underground coal fires in the coal field (Vu and Nguyen 2021b). Therefore, the study of the distribution of LST plays important role in the detection of coal fire risk from remotely sensed data. It has been observed by Mukherjee et al. (2018) that, during the summer season, water bodies have high temperatures, thus affecting the performance of detection of fire risks. This might lead to the false detection of coal fire risks. Therefore, in this study, Landsat-8 TIRS satellite images were collected in the winter season of 2017. Data from **Fig. 2** demonstrates the spatial distribution of land surface temperatures obtained from Landsat-8 TIRS satellite images in the Na Duong coal field, Lang Son province. As can be seen from **Fig. 1**, land surface temperatures ranged from 16.2°C to 35.3°C. The lowest, highest, and mean temperatures were 16.2°C, 35.3°C, and 19.3°C, respectively. What stands out from **Fig. 1** is that low LSTs were mainly concentrated in areas with hills, dense vegetation covers, and on the outside of the coal field. Whereas, high temperatures above 25°C were mainly concentrated in densely populated areas and especially inside the Na Duong coal mining site. Particularly, there is a clear trend that very high land surface temperatures were detected inside areas of the Na Duong coal field. These high LSTs nearby coal fire sites were much higher than those of surrounding environments. This is consistent with the findings in a recent study by Nguyen and Vu (2019b). Another aspect of interestingness about the data in Fig. 1 is that the radiation heat flux was locally concentrated in the Na Duong coal field, especially nearby active coal fire sites. This is also in line with those reported in previous studies (Nguyen and Vu 2019b; Vu and Nguyen 2021b; Vu and Nguyen 2018). This can be judged that underground coal fires were likely to occur in this area.

4.2. Distribution of local Moran's *I* statistic

With the input data of land surface temperatures obtained from Landsat-8 TIRS data in the Na Duong coal field as discussed in the previous section. The local Moran's *I* statistic was employed to discover the spatial patterns of these LSTs. Data from **Fig. 3** demonstrates the spatial distribution of the local Moran's *I* statistic. It can be seen that the study resulted in the values of the local Moran's *I* varying from -0.09 to 62.12. It's minimum, mean, maximum values, and standard deviation of local Moran's *I* index were -0.09, 1.92, 62.12, and 3.14, respectively. From the data in **Fig. 3**, it is apparent that, similar to those obtained from low land surface temperatures, as discussed in section 4.1, low values of local Moran's *I* statistic were mainly detected in the areas outside the coal mining area.

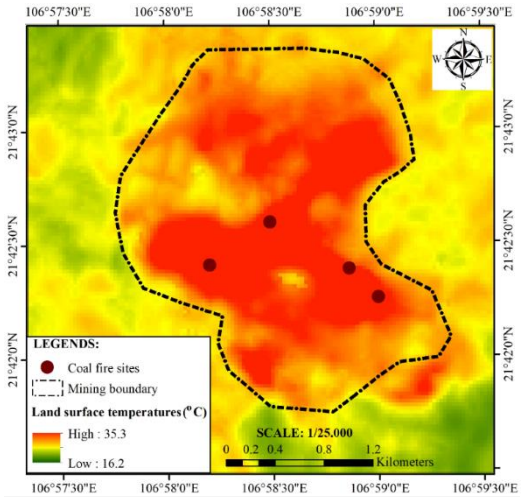

Fig. 2. Spatial distribution of land surface temperatures in the Na Duong coal field.

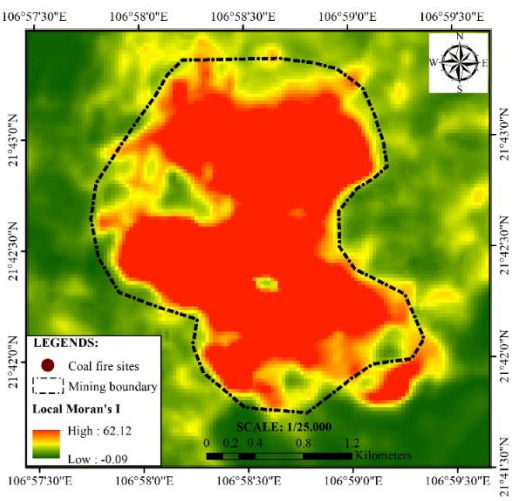

Fig. 3. Spatial distribution of the local Moran's I statistic in the Na Duong coal field.

These areas correspond to different land cover types such as vegetation, bare soil, residential areas, or surface water outside the coal field mining area. The low values of local Moran's *I* statistic represent the spatial clustering of low land surface temperatures (low-low clusters). Whereas, high values of the local Moran's *I* statistic were mainly concentrated in areas with high land surface temperatures above 30°C. These areas were mainly detected in densely populated areas and especially inside the Na Duong coal mining boundary. The most interesting aspect of this figure is that there existed high and very high values of local Moran's *I* inside the Na Duong coal field. These high values of the local Moran's *I* statistic show significant evidence that spatial clustering of high land surface temperatures (high-high clusters) was detected around active coal fires. This proves that areas of high land surface temperatures (thermal anomalies) were concentrated at the time of image acquisition. These high values of Moran's *I* coefficients might be caused due to the existence of the underground coal fires in the coal field.

It can be seen that data from **Fig. 3** can be compared with the data in **Fig. 2** which shows an important difference. The local Moran's *I* statistic highlights the spatial dependence and auto-correlation of land surface temperatures retrieved from Landsat-8 TIRS data. More specifically, the local Moran's statistic highlights areas where high land surface temperatures were highly concentrated (high-high cluster). Typically, although the land surface temperatures were high in the north and northeast of the study area, the local Moran's *I* statistic found there was spatial clustering of high temperatures presenting no concentration of thermal radiation in the north and northwest areas outside the coal field. This is consistent with the fact that no coal fire sites were reported in these areas. Whereas, the most surprising aspect of the data in Fig. 3 is that the local Moran's statistic well detected a high degree of spatial dependence or spatial auto-correlation in areas of high land surface temperatures around coal mine fire points within the mining area. Additionally, the histogram for the local Moran's statistic shows that the data of land surface temperatures does not follow the normal distribution. The distribution of the local Moran's *I* statistic is rather right-skewed due to the existence of high and very high values of the local Moran's *I* statistic. A large number of the local Moran's *I* values were found in the range of 0 to 4. The values of local Moran's *I* which are greater than 10 presenting high land surface temperatures were highly concentrated. This proves that there existed high risk of the underground coal fires in the coal mining area in the Na Duong coal field.

4.3. Analysis of coal fire risk areas

As discussed in the previous section, the distribution of the local Moran's *I* statistic is strongly right-skewed due to the existence of high and very high land surface temperatures caused by active coal fires in the coal field. The anomalies of the local Moran's *I* statistic reflect the high degree of concentration of high land surface temperatures or spatial clustering of high temperatures (high-high clusters). It is, therefore, these anomalies were identified by setting the MEAN+2*SDEV, MEAN+3*SDEV, and MEAN+4*SDEV formulas as thresholds on the local Moran's *I* coefficient. With the values of the mean and standard deviation of 1.92 and 3.14, three different thresholds of 8.74, 12.15, and 15.56 were successfully determined for the local Moran's *I* statistic, respectively. In this case, based on these three thresholds, the areas of coal fire risk areas were delineated and ranked, accordingly, as follows: (i) no risk, if $I_i < 8.74$; (ii) low risk, if $8.74 \leq I_i < 12.15$; (iii) moderate risk, if $12.15 \leq I_i < 15.56$; and (iv) high risk, $I_i \geq 15.56$. These areas of coal fire risk levels were then validated using four active coal fire sites collected from the field survey at the time of image acquisition. From the data in **Fig. 4**, it can be seen that there was a high degree of spatial correlation or good conformity between the areas of coal fire risks and active coal fire sites (high-high clusters). Particularly, coal fire areas at high-risk level were detected around the known coal fire sites. As data in **Fig. 4** shows the further away from the active coal fires, the lower the risks of fires. This is consistent with those reported in previous studies (Vu and Nguyen 2021b; Vu and Nguyen 2018). Additionally, it can be seen that coal fire areas from **Fig. 4** can be compared with those in **Fig. 5** which shows good conformity, especially for coal fire risks at the moderate level. Thus, it can be concluded that these results prove the effectiveness and high accuracy of the proposed method.

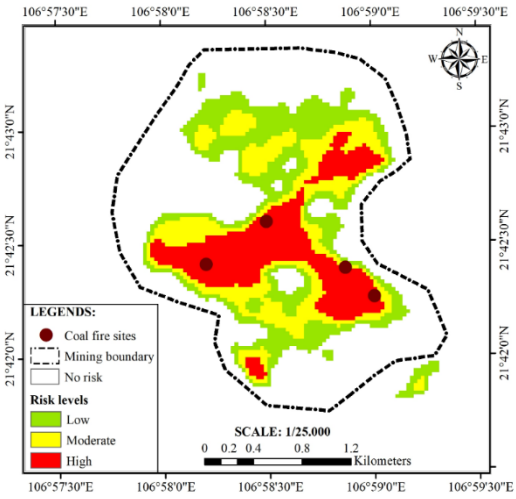

Fig. 4. Coal fire risk areas delineated using the local Moran's *I* in the Na Duong coal field.

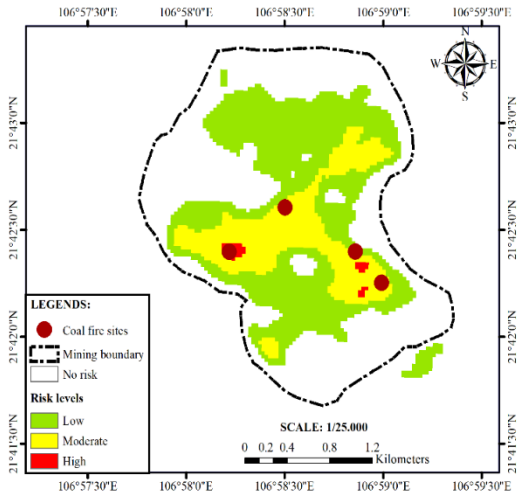

Fig. 5. Coal fire risk areas delineated using the hot spot analysis in the Na Duong coal field.

Data from **Fig. 4** illustrates the spatial distribution of coal fire risk areas in the Na Duong coal field in the winter season of 2017. It can be seen that coal fire risks at moderate and high levels were mainly detected in the center of the coal field. Whereas, coal fire risks at the low level were found around areas of risk at moderate and high levels in the northern part of the coal field. There was almost no risk of underground coal fires in such land cover types as forests, water surfaces, and densely populated areas where the low degree of spatial auto-correlation was identified in areas of low land surface temperatures. Additionally, underground coal fire risks at low, moderate, and high levels were mainly detected inside the coal mining area of Na Duong. Most importantly, coal fire risks at the high level were mainly concentrated near known coal fire sites (as shown in **Fig. 4**). Besides that, the local Moran's *I* anomalies caused by high land surface temperatures were also found in the southeast region of the study area. However, these were false anomalies caused by the high density of the population.

5. CONCLUSIONS

In this study, a method for the delineation of coal fire risk areas from Landsat-8 TIRS data was proposed. Land surface temperatures were first retrieved from the Landsat-8 TIRS data using the radiative transfer equation. The degree of spatial autocorrelation among land surface temperatures was then identified with the help of the local Moran's *I* statistic. Thermal-related anomalies for the delineation of coal fire risk areas were finally identified by setting the MEAN+2*SDEV, MEAN+3*SDEV, and MEAN+4*SDEV formulas as thresholds on the local Moran's *I* statistic. The results of this study show that coal fire risks at moderate and high levels were mainly detected in the center of the coal field. The higher values of local Moran's *I* statistic, the higher levels of coal fire risk. These findings suggest that Landsat-8 TIRS data and the proposed method can effectively delineate coal fire risk areas.

AUTHOR CONTRIBUTIONS

Tien-thanh NGUYEN conceived and designed the study. Anh-huy HOANG and Thi-thu-huong PHAM collected the data. Tien-thanh Nguyen and Danh-tuyen VU performed image processing and wrote the manuscript. All authors discussed the results, and implications and commented on the manuscript at all stages.

ACKNOWLEDGMENT

This study is sponsored and financed by the Ministry-level Scientific and Technological Key Programs of Ministry of Natural Resources and Environment of Viet Nam "Application of thermal infrared remote sensing and GIS for mapping underground coal fires in Quang Ninh coal basin" (Grant number TNMT.2017.08.06).

REFERENCES

Anselin L (1995) Local indicators of spatial association—LISA. Geographical analysis 27 (2):93-115

Barsi JA, Barker JL, Schott JR An atmospheric correction parameter calculator for a single thermal band earth-sensing instrument. In: Geoscience and Remote Sensing Symposium, 2003. IGARSS'03. Proceedings. 2003 IEEE International, 2003. IEEE, pp 3014-3016. doi:http://dx.doi.org/10.1109/IGARSS.2003.1294665

Chen G, He Y, De Santis A, Li G, Cobb R, Meentemeyer RK (2017) Assessing the impact of emerging forest disease on wildfire using Landsat and KOMPSAT-2 data. Remote Sensing of Environment 195:218-229

Du X, Cao D, Mishra D, Bernardes S, Jordan TR, Madden M (2015) Self-adaptive gradient-Based thresholding method for coal fire detection using ASTER thermal infrared data, part I: methodology and decadal change detection. Remote sensing 7 (6):6576-6610

Ducrocq S, Benammi M, Chavasseau O, Chaimanee Y, Suraprasit K, Pha PD, Phuong VL, Phach PV, Jaeger J-J (2015) New anthracotheres (Cetartiodactyla, Mammalia) from the Paleogene of northeastern Vietnam: biochronological implications. Journal of Vertebrate Paleontology 35 (3):e929139

Ellyett C, Fleming AW (1974) Thermal infrared imagery of the Burning Mountain coal fire. Remote Sensing of Environment 3 (1):79-86

Greene GW, Moxham RM, Harvey AH (1969) Aerial infrared surveys and borehole temperature measurements of coal mine fires in Pennsylvania. Remote Sensing of Environment, VI:517

Hoang VT (2005) Working environment and health of workers in Na Duong coal mine, Lang Son province. Journal of Preventive Medicine:65-69

Huo H, Jiang X, Song X, Li Z-L, Ni Z, Gao C (2014a) Detection of coal fire dynamics and propagation direction from multi-temporal nighttime Landsat SWIR and TIR data: A case study on the Rujigou coalfield, Northwest (NW) China. Remote sensing 6 (2):1234-1259

Huo H, Jiang X, Song X, Ni Z, Liu L (2014) Coal fires dynamics detection over Rujigou coalfield, Ningxia, NW China. In: Geoscience and Remote Sensing Symposium (IGARSS), 2014 IEEE International, 2014b. IEEE, pp 4512-4515. doi:https://dx.doi.org/10.1109/IGARSS.2014.6947495

Huo H, Ni Z, Gao C, Zhao E, Zhang Y, Lian Y, Zhang H, Zhang S, Jiang X, Song X (2015) A study of coal fire propagation with remotely sensed thermal infrared data. Remote Sensing 7 (3):3088-3113. doi:https://dx.doi.org/10.3390/rs70303088

Knuth W, Fisher Jr W, Stingelin R (1968) Detection, delineation and monitoring of subsurface coal fires by aerial infrared scanning. Geographer HRB-Singer, Inc, a subsidiary of the Singer Company, state College, Pennsylvania, USA:877-881

Kowe P, Mutanga O, Odindi J, Dube T (2019) Exploring the spatial patterns of vegetation fragmentation using local spatial autocorrelation indices. Journal of Applied Remote Sensing 13 (2):024523-024523

Kuenzer C, Zhang J, Li J, Voigt S, Mehl H, Wagner W (2007) Detecting unknown coal fires: synergy of automated coal fire risk area delineation and improved thermal anomaly extraction. International Journal of Remote Sensing 28 (20):4561-4585

Künzer C (2014) Remote and in situ mapping of coal fires: case studies from China and India. Coal and Peat Fires: A Global Perspective Volume 3: Case Studies–Coal Fires 3:57-93

Mishra N, Haque M, Leigh L, Aaron D, Helder D, Markham B (2014) Radiometric cross calibration of Landsat 8 operational land imager (OLI) and Landsat 7 enhanced thematic mapper plus (ETM+). Remote Sensing 6 (12):12619-12638

Mukherjee J, Mukherjee J, Chakravarty D Detection of coal seam fires in summer seasons from Landsat 8 OLI/TIRS in Dhanbad. In: Computer Vision, Pattern Recognition, Image Processing, and Graphics: 6th National Conference, NCVPRIPG 2017, Mandi, India, December 16-19, 2017, Revised Selected Papers 6, 2018. Springer, pp 529-539

Nguyen TT (2017) Use of Moran's I and robust statistics to separate geochemical anomalies in Jiurui area (Southeast China). Bulletin Of The Mineral Research and Exploration 156 (156):179-192

Nguyen TT, Vu DT, Nguyen TLH (2016) Spatial cluster and outlier identification of geochemical association of elements: A case study in Juirui copper mining area. Bulletin of the Mineral Research and Exploration 153 (153):159-167

Nguyen TT, Vu TD (2019a) Identification of multivariate geochemical anomalies using spatial autocorrelation analysis and robust statistics. Ore Geology Reviews 111:102985

Nguyen TT, Vu TD (2019b) Use of hot spot analysis to detect underground coal fires from Landsat-8 TIRS data: A case study in the Khanh Hoa coal field, north-east of Vietnam. Environment and Natural Resources Journal 17 (3):1-10

Pubellier M, Rangin C, Phach PV, Que BC, Hung D, Sang C (2003) The Cao Bang-Tien Yen Fault: Implications on the relationships between the Red River Fault and the South China Coastal Belt. Advances in Natural Sciences 4 (4):347-361

Rabchevsky G (1972) Determination from Available Satellite and Aircraft Imagery of the Applicatility of Remote Sensing Techniques to the Detection of Fires Burning in Abandoned Coal Mines and Unmined Coal Deposits Located in North Central Wyoming and Southern Montana. Contract No SO 211087

Singh A, Raju A, Pati P, Kumar N (2017) Mapping of Coal Fire in Jharia Coalfield, India: a Remote Sensing Based Approach. Journal of the Indian Society of Remote Sensing 45 (2):369-376. doi:https://doi.org/10.1007/s12524-016-0590-5

Sobrino JA, Jiménez-Muñoz JC, Sòria G, Romaguera M, Guanter L, Moreno J, Plaza A, Martínez P (2008) Land surface emissivity retrieval from different VNIR and TIR sensors. IEEE Transactions on Geoscience and Remote Sensing 46 (2):316-327. doi:https://dx.doi.org/10.1109/TGRS.2007.904834

Song Z, Kuenzer C (2017) Spectral reflectance (400–2500 nm) properties of coals, adjacent sediments, metamorphic and pyrometamorphic rocks in coal-fire areas: A case study of Wuda coalfield and its surrounding areas, northern China. International Journal of Coal Geology 171:142-152

Tiefelsdorf M (2002) The saddlepoint approximation of Moran's I's and local Moran's Ii's reference distributions and their numerical evaluation. Geographical analysis 34 (3):187-206

Vu D-t, Nguyen T-t (2021a) Spatial pattern of land surface temperatures and its relation to underground coal fires in the Khanh Hoa Coal Field, North-East of Vietnam. Arabian Journal of Geosciences 14 (3):1-15

Vu D-t, Nguyen T-t (2021b) Spatial pattern of land surface temperatures and its relation to underground coal fires in the Khanh Hoa Coal Field, North-East of Vietnam. Arabian Journal of Geosciences 14 (3):145

Vu TD, Nguyen TT (2018) Spatio-temporal changes of underground coal fires during 2008–2016 in Khanh Hoa coal field (North-east of Viet Nam) using Landsat time-series data. Journal of Mountain Science 15 (12):2703-2720

Wysocka A (2009) Sedimentary environments of the Neogene basins associated with the Cao Bang–Tien Yen Fault, NE Vietnam. Acta Geologica Polonica 59 (1):45-69